ISSN No:-2456-2165

Enhancing Aerodynamic Performance of Vertical Stabilizers through Leading Edge Modifications: A CFD Analysis

Muhammad Koder[1]*
1Graduate Facility of Saint Louis University, USA

Abstract:- This research paper presents a meticulous investigation that was conducted by the authors for the effects of variable length V-shaped leading-edge morphing on drag reduction in NACA 0012 vertical stabilizers. This study aimed at enhancing the aerodynamic performance of these critical aircraft components under transonic conditions. Employing computational fluid dynamics (CFD) analysis, the researchers explored the potential of V-shaped leading-edge morphing in improving the overall aerodynamic efficiency. Through systematic simulations and rigorous analysis, the researchers were able to provide valuable insights into the effects of different leading-edge lengths and angles of attack on drag coefficients and lift performance. While the outcomes did not yield a significant reduction in drag, this research significantly contributes to the ongoing exploration of innovative techniques in aerodynamics for mitigating drag penalties in vertical stabilizers.

Keywords:- *NACA 0012, Vertical stabilizer, Edge morphing, Aerodynamics, CFD, Drag.*

I. INTRODUCTION

Efficient aerodynamic design plays a pivotal role in advancing aerospace engineering, with ongoing efforts focused on enhancing the aircraft's performance and fuel efficiency (IPCC, 1999). Among the various components influencing the aerodynamic drag, the vertical stabilizer of an aircraft's tail poses a significant challenge (NASA Glenn Research Center). It is not only vital for stability and control, but also contributes to substantial drag forces, particularly during transonic flight encountered by commercial air vehicles (Leishman, 2023). Therefore, addressing the drag penalties associated with vertical stabilizers necessitates the exploration of novel approaches inspired by nature's remarkable adaptations. In this study, our objective was to investigate the effects of variable length V-shaped leading-edge morphing on drag reduction in NACA 0012 vertical stabilizers. The NACA 0012 airfoil, widely adopted for vertical stabilizers due to its symmetrical profile, served as the representative model for this research (Wood, 2022).

The central hypothesis posited that the implementation of a V-shaped configuration, featuring variable lengths, in the leading edge of the NACA 0012 airfoil holds the potential to yield a substantial reduction in pressure drag and improved aerodynamic performance of vertical stabilizers. To rigorously test this hypothesis, a comprehensive computational fluid dynamics (CFD) analysis was conducted employing ANSYS Fluent, a well-established CFD software, known for its proven accuracy and reliability (ANSYS, 2021). In this context, this research embarked on a meticulous investigation that was aimed at exploring the feasibility and potential benefits of incorporating leading edge modifications inspired by biomimicry principles. In this research, the researchers were specifically inspired from the hydrodynamic attributes observed in the sailfish (Istiophorus platypterus) which is recognized for its exceptional prowess and swiftness in aquatic environments. Thus, it served as an intriguing source of inspiration for enhancing the aerodynamic performance of vertical stabilizers (Norman, 1929; Sagong et al., 2013).

The current study primarily focused on transonic conditions which are characterized by shockwaves and compressibility effects which pose unique challenges in aerodynamic analysis (James, 1986). By means of computational fluid dynamics (CFD) simulations, we aimed to comprehensively capture the intricate flow phenomena encompassing the NACA 0012 vertical stabilizers (Airfoil Tools, a) and evaluate the repercussions of V-shaped leading-edge morphing at varying lengths. In order to establish the robustness and veracity of these CFD simulations, we undertook a meticulous validation procedure encompassing a rigorous comparison between the computed lift and drag coefficients and well-documented experimental and computational data pertinent to the NACA 0012 airfoil under transonic conditions (Holst, 1988: El Maani et al., 2018). The compelling concurrence observed between the simulation results and the validated values served to affirm the soundness and trustworthiness of the current research's analytical approach.

We employed sophisticated mesh generation techniques to achieve accurate predictions and convergence of results. Through systematic refinement, we achieved mesh independence and effectively captured the intricate flow field details surrounding the NACA 0012 vertical stabilizers. This meticulous approach facilitated a comprehensive analysis of the effects of variable length V-shaped leading-edge morphing, enabling a precise evaluation of its impact on the aerodynamic performance. Furthermore, we investigated the impact of variable angles of attack on the drag coefficient and lift performance of the NACA 0012 vertical stabilizers. Multiple simulations were conducted with spanning angles of attack from 0 to 5 degrees (Haygood, 2022) and replicating the vertical stabilizer's role in generating lift during different flight conditions especially when the aircraft was under One Engine Inoperative (OEI) conditions.

The objective of this research paper was to provide an extensive analysis of the effects resulting from variable length V-shaped leading-edge morphing in NACA 0012 vertical stabilizers at varying angles of attack. Thorough this investigation, we aimed to contribute to the advancement of knowledge and understanding in the field of aerodynamic design. This study seeks to expand the current understanding of the aerodynamic performance of vertical stabilizers, specifically exploring the potential benefits and implications of incorporating variable length V-shaped leading-edge morphing.

II. METHODOLOGY

This experiment investigated the effects of variable length V-shaped leading-edge morphing on the aerodynamic performance of NACA 0012 vertical stabilizers during cruising conditions. By utilizing advanced computational tools, turbulence modelling, accurate meshing techniques, and controlling y+ values, this methodology contributes to a deeper understanding of the aerodynamic performance of vertical stabilizers in cruising flight where the fluid become compressible. The technical soundness and meticulousness of this methodology ensured its relevance and reliability in the field of fluid and aerodynamics, paving the way for further advancements in the design and optimization of vertical stabilizers. The methodology encompassed the following key steps and considerations, ensuring scientific rigor and accuracy in the analysis.

A. Geometry and Mesh Generation

The geometric model of the NACA 0012 vertical stabilizers was constructed using the Airfoil Tools website (Airfoil Tools, b) while the fluid domain was constructed using Ansys Design Modeler, which accurately represented the airfoil's shape and dimensions. Then, a structured mesh generation technique was employed to discretize the computational domain around the NACA 0012 vertical stabilizers, ensuring precise capturing of the flow features and reducing numerical errors (El Maani et al., 2018). After this, the mesh was refined and optimized to achieve grid independence and accurately resolve the flow structures around the airfoil. Finally, the y+ approach was utilized to capture the boundary layer characteristics near the airfoil surface. The maximum y+ value was carefully controlled below 5 to accurately resolve the viscous sublayer profile (LEAP CFD Team, 2012; 2020).

B. Computational Fluid Dynamics Simulations

The simulations were performed using a validated commercial CFD solver named ANSYS Fluent. The governing equations for fluid flow, including the continuity, momentum, and energy equations, were solved using a time-accurate approach to capture the effects during cruising conditions. Appropriate boundary conditions, such as pressure far field, atmospheric conditions, and aircraft configuration parameters, were applied to simulate realistic cruising scenarios at transonic condition at mach number 0.7 (Thomas and Salas, 1986; El Maani et al., 2018). The effects of variable length V-shaped leading-edge morphing were incorporated into the airfoil geometry, thus, enabling the evaluation of their impact on the aerodynamic performance of the vertical stabilizers during the transonic condition.

C. Turbulence Modelling

A suitable turbulence model was selected to accurately capture the turbulent behavior around the airfoil during cruising conditions. The k-ω Shear Stress Transport (SST) model, known for its effectiveness in capturing turbulence characteristics, was employed in the simulations (ANSYS FLUENT, 12.0; Menter et al., 1.0). The model incorporated advanced turbulence closure equations, allowing for accurate predictions of flow separation, drag, lift, and boundary layer characteristics.

D. Simulation Analysis and Results

The CFD simulations generated a wealth of data, including pressure distribution, velocity profiles, skin friction coefficients, and boundary layer profiles. Post-processing and analysis techniques were applied to extract meaningful insights from these simulation results. The boundary layer characteristics, captured using the y+ approach, were analyzed to assess the accuracy of the simulation in resolving the viscous sublayer profile (Menter et al., 1.0). Key aerodynamic parameters, such as the effect of V-shaped leading-edge morphing on drag reduction, lift enhancement, and flow characteristics, were meticulously evaluated and quantified. Statistical analyses, visualization tools, and comparison with relevant literature data, were employed to validate and verify the simulation results.

III. RESULTS

A. Evaluation of Different Design Configurations

A meticulous data collection process was carried out, and the obtained results were organized and presented in Table 1. This table serves as a valuable resource for researchers and practitioners in the field, offering a comprehensive overview of the aerodynamic characteristics observed across different system configurations and angles of attack. By analyzing the data within this table, it becomes possible to discern the relationships and dependencies between the angles of attack, configuration variations, and their corresponding effects on the identified aerodynamic parameters.

The comparative analysis depicted in Fig. 1 provides insights into the aerodynamic performance of various configurations at different angles of attack (AOA). As expected, an increase in the length of the V-shaped nose resulted in a larger drag coefficient due to the corresponding increase in the chord length, the relationship between the drag and chord length are directly proportional quantities. Conversely, a reduction in the length of the V-shaped nose brought the drag coefficient closer to that of the original NACA 0012 base configuration. Notably, the configuration with a length of 23.33 mm, representing 2.33% extra of chord length, configuration, exhibited slightly improved drag reduction. This figure effectively showcases the variations in drag performance across the seven different configurations, providing valuable insights for the analysis of aerodynamic behavior in this study.

ISSN No:-2456-2165

Table 1: Observed parameters for different lengths

NACA 0012							
Degree	CD	Lift	Drag Force (N)	Skin_friction	Dyn_pressure(N)	Total pressure(N)	Wall_shear(N)
0 Degree	0.00777	0.0033	194.59	0.00285	440.64	67010.82	71.37
1 Degree	0.00796	0.14876	199.446	0.00284	437.146	66916.57	71.107
2 Degree	0.00876	0.303	219.374	0.0028	420.965	66602.773	70.1617
3 Degree	0.01317	0.4513257	329.957	0.00269	389.83884	66062.984	67.559
4 Degree	0.023	0.57354	576.2117	0.002543	351.09341	65435.84	63.667
5 Degree	0.0349	0.62253	874.127	0.002329	316.6226	64985.82	58.3223
333.33 Configuration							
0 Degree	0.0138	0	345.85	0.002754	251.296	69592.5	68.96
1 Degree	0.0151	0.1763	378.75	0.002546	230.503	69474.2	63.747
2 Degree	0.01935	0.311	484.7	0.002248	196.404	69213.82	56.307
3 Degree	0.0296	0.439	674.18	0.00202	171.19	68852.71	50.695
4 Degree	0.0372	0.542215	932.85	0.001828	151.555	68449.58	45.787
5 Degree	0.05	0.605703	1253.92	0.00166	139.322	68056.29	41.65
233.33 Configuration							
0 Degree	0.00831	0	208.105	0.002748	195.72011	69116.93	68.8232
1 Degree	0.00909	0.158928	227.81	0.00257	184.902	68993.6	64.515
2 Degree	0.01198	0.2925	300.08	0.00237	166.8653	68690.58	59.487
3 Degree	0.017	0.4124	426.658	0.00218	149.928	68278.95	54.695
4 Degree	0.02412	0.516644	603.878	0.00199	132.3775	67806	49.851
5 Degree	0.0336	0.59277	841.059	0.0018	117.444	67324.99	45.087
133.33 Configuration							
0 Degree	0.00797	0	199.595	0.00278	195.6552	68453.07	69.604
1 Degree	0.00849	0.1536	212.574	0.00264	185.4736	68329.97	66.2166
2 Degree	0.01048	0.2858	262.476	0.00247	169.8775	68056.88	61.8469
3 Degree	0.0144	0.4342	360.668	0.002299	152.098	67566.391	57.5752
4 Degree	0.0141	0.4039	529.065	0.002287	153.2856	67657.27	57.2742
5 Degree	0.02616	0.58198	655.155	0.001912	123.242	66738.14	47.874
58.33 Configuration							
0 Degree	0.00774	0	193.95	0.002799	200.138	67712.25	70.0864
1 Degree	0.008079	0.151	202.3	0.002718	192.66	67607.56	68.0729
2 Degree	0.00942	0.292	235.861	0.002585	177.76	67314.39	64.74
3 Degree	0.01317	0.422	329.873	0.0024	156.56	66857.7	60.23
4 Degree	0.01991	0.5281	498.653	0.0022	137.487	66354.88	55.113
5 Degree	0.0279	0.5924	699.63	0.001997	125.4	65919.66	50
33.33 Configuration							
0 Degree	0.00767	0	192.256	0.002798	189.632	67344.961	70.056
1 Degree	0.00794	0.1509	198.92	0.002739	183.929	67243.58	68.595
2 Degree	0.009058	0.2961	226.802	0.00262	170.603	66948.22	65.7447
3 Degree	0.01313	0.43133	328.79	0.002453	151.319	66474.023	61.4219
4 Degree	0.021413	0.54016	536.141	0.00247	133.75	65945.16	56.264
5 Degree	0.0316	0.5887	791.224	0.00202	121.839	65548.09	50.808
23.33 Configuration							
0 Degree	0.00764	0	191.515	0.00295	157.081	67144.9	70.003
1 Degree	0.007862	0.1522	196.864	0.00274	152.655	67043.51	68.654
2 Degree	0.00887	0.3	222.275	0.00264	142.977	66745.41	66.107
3 Degree	0.01313	0.4365	328.877	0.00246	126.413	66269.81	61.774
4 Degree	0.0222	0.5554	557.145	0.00227	111.244	65699.9	57.018
5 Degree	0.0329	0.5956	823.78	0.00205	100.241	65324.75	51.548

The lift coefficient for the zero AOA for all the configurations was zero. The lift started to generate as we started inducing the AOA for the configurations. As we increased the length of the V-shape configuration, the lift increased for only one- and two-degree configurations. Then the original configuration NACA 0012 became the superior in lift generation in transonic condition.

ISSN No:-2456-2165

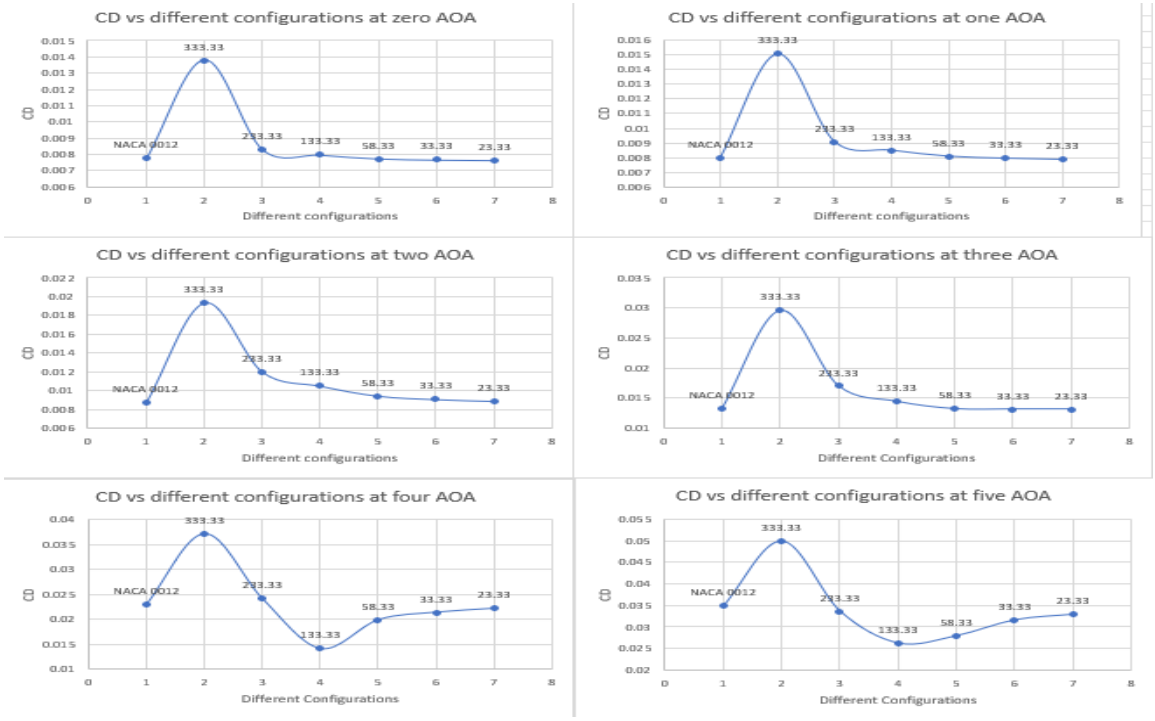

Fig. 1: Drag coefficient at different AOA for different configurations

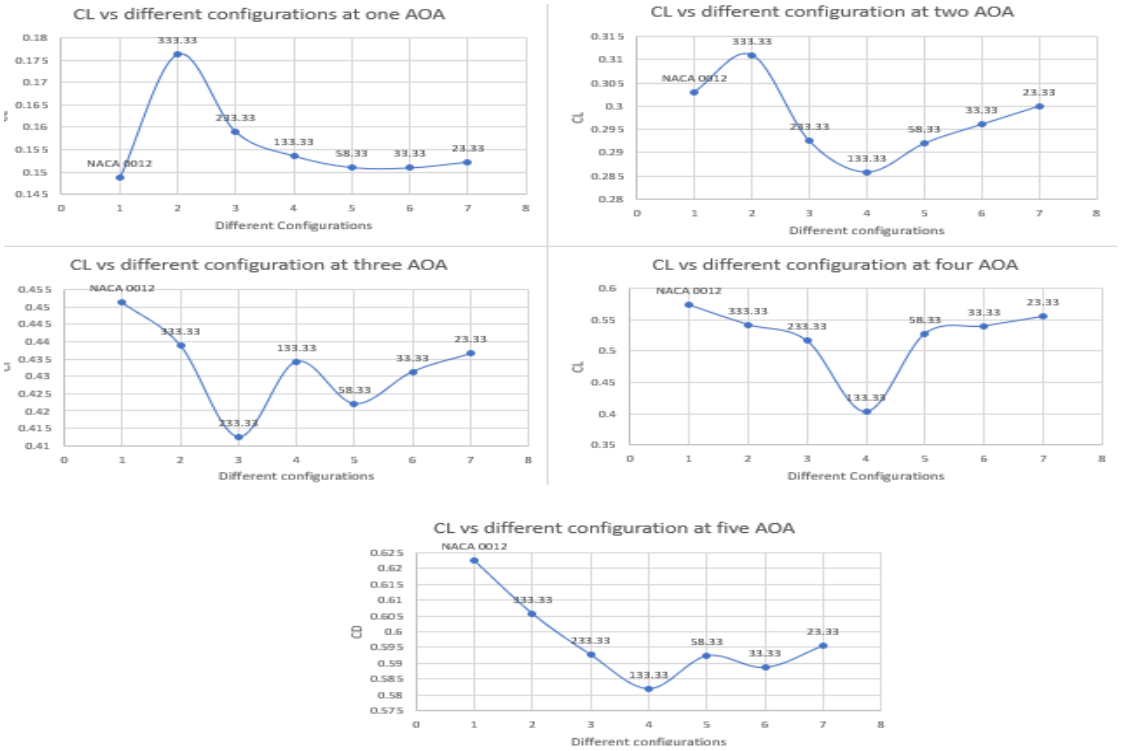

Fig. 2: Lift coefficient at different AOA for different configurations

The presented figure offers valuable insights into the behavior of the skin friction coefficient in a transonic flow regime at Mach 0.7. The plotted graphs illustrate that, except for the 23.33 mm configuration at zero angle of attack at zero AOA with 3.86% decrease in drag, the NACA 0012 airfoil consistently exhibited the highest skin friction coefficient along the airfoil wall. Conversely, the longest V-shaped configurations consistently demonstrated the lowest skin friction coefficients. It is worth noting that in transonic conditions, the form drag became the dominant factor influencing the overall drag, while in laminar flow regimes, the skin friction coefficient played a crucial role and significantly contributed to the total drag experienced by the airfoil. These observations provided valuable insights into the relationship between the V-shaped leading-edge configurations and the skin friction coefficient, aiding in a better understanding of aerodynamic performance in transonic flows and the factors influencing drag characteristics.

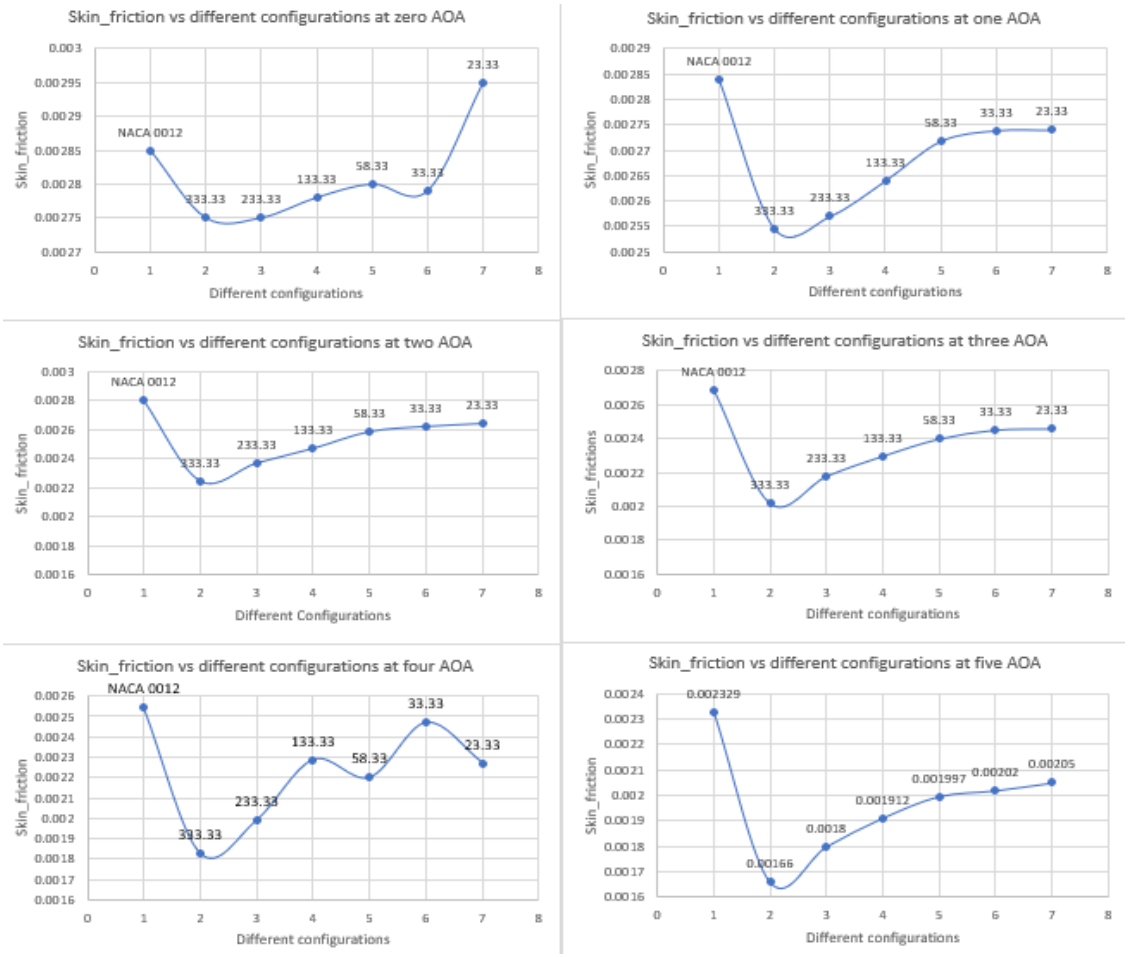

Fig. 3: Skin friction coefficients at the wall for different AOA

B. Analysis of Flow Characteristics

The simulations conducted in this study provided detailed insights into the flow behavior and characteristics influenced by the NACA 0012 airfoil and the V-shaped leading-edge morphing. Through the careful analysis of velocity profiles, boundary layer profiles, and other relevant flow visualization results, a comprehensive understanding of the flow patterns and dynamics in the transonic fluid regime was achieved. The examination of these flow visualization outputs revealed notable phenomena, particularly regarding the occurrence of flow separation and the formation of shock waves.

As the length of the V-shaped leading-edge increased, the onset of flow separation became more pronounced especially at the front of the V shape. This observation suggested that the morphing technique influenced the flow field and affected the flow attachment along the airfoil surface. Additionally, at a specific angle of attack of 3 degrees, the simulations exhibited the generation of shock waves, which contributed to an increase in drag. The presence of shock waves in the flow field is known to induce substantial aerodynamic drag due to the abrupt change in flow properties across the shock front.

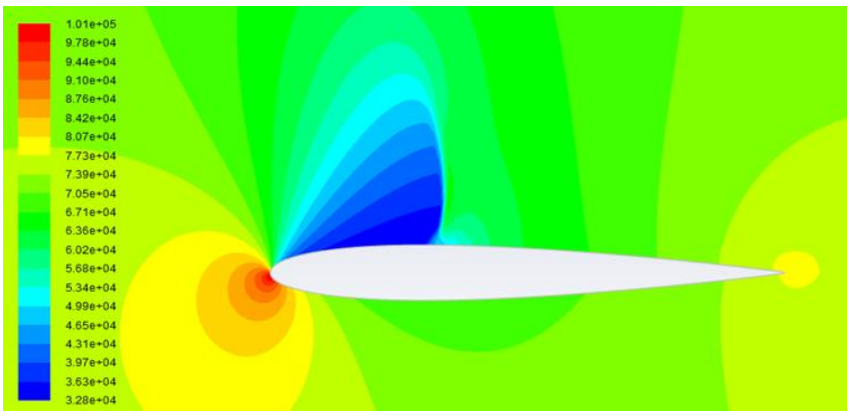

Fig. 4: Pressure contour at 4-degree NACA 0012

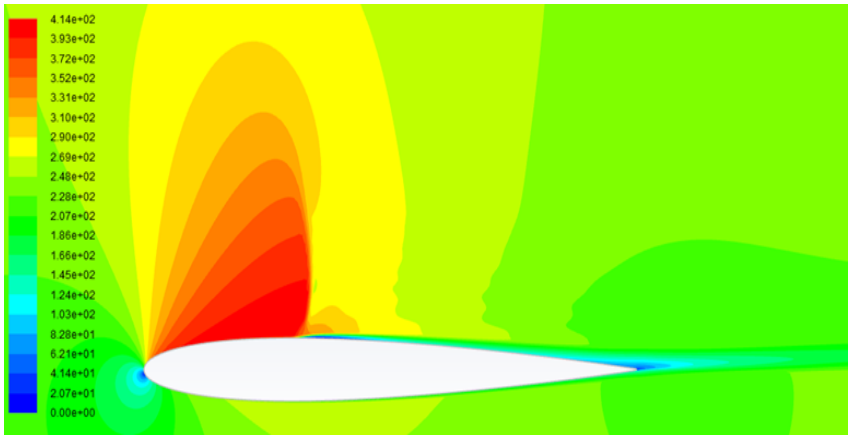

Fig. 5: Velocity contour at 4-degree NACA 0012

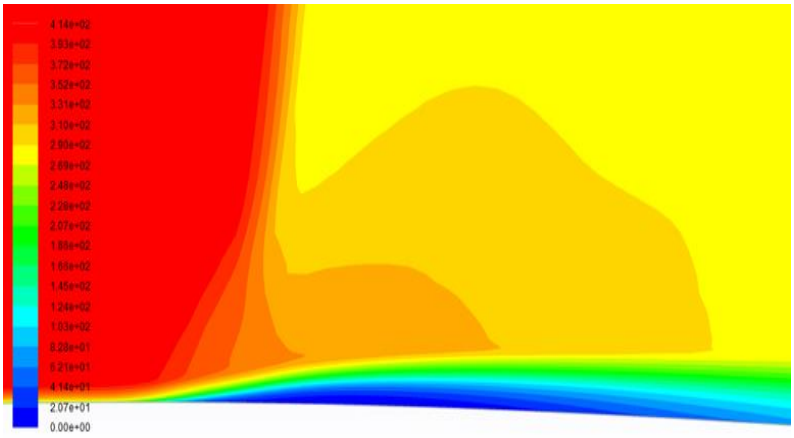

Fig. 6: Velocity contour at 4-degree NACA 0012 separation and shock wave

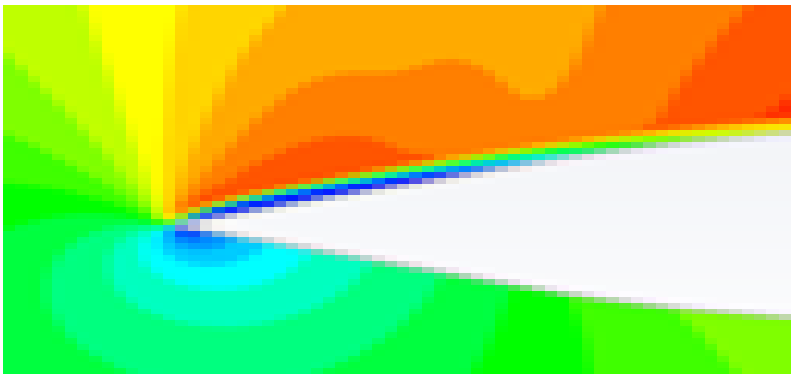

Fig. 7: Separation at the V shape at 4-degree AOA

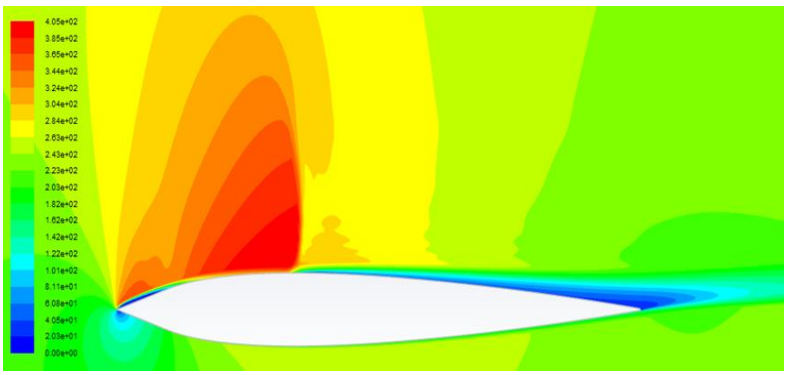

Fig. 8: Velocity contour for 58.33 mm 5-degree AOA configuration V-shape

IV. DISCUSSION

These findings underscore the significance of considering flow phenomena and characteristics when evaluating the effectiveness of the V-shaped leading-edge morphing approach. Shock waves are a result of abrupt changes in flow properties (Nejati and Mazaheri, 2016), including pressure, density, and velocity, which occur when airflow experiences rapid acceleration or deceleration. These shock waves have a significant impact on drag due to various factors. Firstly, shock waves cause a notable increase in static pressure behind the shock front, contributing to overall drag. Secondly, the abrupt deceleration of airflow across shock waves leads to the conversion of kinetic energy into thermal energy, further augmenting drag. Additionally, shock waves can induce flow separation, where the airflow detaches from the airfoil surface, resulting in an enlarged wake region and increased pressure drag. Moreover, shock waves influence the behavior of the boundary layer, leading to boundary layer separation and heightened skin friction drag (Neuenhahn and Olivier, 2006).

In the specific context of the V-shaped leading-edge morphing discussed earlier, the observed increase in drag at an angle of attack of 3 degrees and up can be attributed to the formation and interaction of shock waves. The flow separation (Placek and Ruchala, 2018) induced by the V-shaped leading-edge morphing especially at the tip of the V shape likely generated shock waves that contributed to the overall drag experienced by the airfoil. An in-depth analysis of shock wave behavior and its influence on drag is crucial for optimizing aerodynamic systems to ensure efficient and high-performance operations in transonic and supersonic flight regimes (Jang et al., 2021). By understanding and managing the effects of shock waves, researchers and practitioners can develop strategies to mitigate drag and enhance overall aerodynamic performance.

Flow separation is critical phenomenon associated with drag. When adverse pressure gradients (Tanarro et al., 2019) or unfavorable flow conditions are present, the airflow detaches from the airfoil surface, resulting in flow separation. This separation creates a larger wake region behind the airfoil and increases the pressure drag. The V-shaped leading-edge morphing, with its modification of the airfoil's geometry, can induce flow separation due to adverse pressure gradients created along the V-shaped region. This flow separation contributes to an additional increase in drag, particularly at certain angles of attack where the adverse pressure gradients are more pronounced.

The relationship between shock waves, flow separation, and the V-shaped leading-edge morphing is intricately intertwined. The presence of shock waves can exacerbate flow separation, as the interaction between the shock wave and the separated flow further destabilizes the boundary layer (Clemens and Narayanaswamy, 2014). This interaction leads to increased turbulent flow, larger separation regions, and heightened drag. Consequently, the V-shaped leading-edge morphing, which introduces modifications to the airfoil geometry, can influence the formation and behavior of shock waves and the occurrence of flow separation.

Understanding the impact of shock waves, flow separation, and the V-shaped leading-edge morphing on drag is crucial for optimizing aerodynamic performance. Through careful design considerations and flow control strategies, engineers aim to minimize shock wave formation, reduce flow separation, and mitigate associated drag. Various techniques, such as shock wave control devices, boundary layer control mechanisms, and optimal airfoil shaping as per this study, are employed to manage these phenomena and optimize aerodynamic performance (Sundharasan et al., 2022).

The comprehensive understanding of shock wave behavior, flow separation characteristics, and the influence of the V-shaped leading-edge morphing provides valuable insights to the fluid community. By unraveling the complex interactions and their effects on drag, researchers and practitioners can develop advanced aerodynamic design and optimization strategies. This knowledge is pivotal for enhancing the efficiency, performance, and sustainability of aerodynamic systems, especially in transonic and supersonic flight regimes (Liem et al., 2015). The continuous exploration of these phenomena will undoubtedly lead to the development of more efficient and high-performance aircraft and contribute to the advancement of fluid dynamics research.

In the pursuit of optimizing aerodynamic performance, this study was seeking optimizing airfoil shaping, which are employed. However, it is important to acknowledge certain limitations and uncertainties associated with the results obtained in this study (Martins, 2022).

The simulations and analyses conducted in this research are based on specific assumptions and simplifications, which may introduce uncertainties. Further validation through wind tunnel testing or flight tests is necessary to verify and refine the findings. Additionally, the effectiveness of the optimal airfoil shaping may vary in real-world applications due to factors such as operating conditions, aircraft configurations, and aerodynamic constraints. The study primarily focused on the transonic regime and a specific airfoil design NACA 0012 and generalizing the findings to different scenarios may require additional investigations. Exploring the effects of varying parameters, such as Mach number and angle of attack, can provide further insights into optimal airfoil shaping.

To address these limitations, future research directions may involve conducting more extensive experimental studies, incorporating more realistic flow conditions and configurations. Advanced computational techniques, such as high-fidelity simulations and machine learning algorithms, can also be employed to refine the optimization process. Considering the multidisciplinary aspects of airfoil design, such as structural considerations and manufacturing constraints, can provide a comprehensive understanding of optimal airfoil shaping and its impact on aircraft performance especially the drag and lift. By addressing these

limitations, conducting further investigations, and refining methodologies, we can enhance our understanding of airfoil optimization and pave the way for more efficient and high-performance aerodynamic systems.

V. CONCLUSION

This research aimed to optimize aerodynamic performance through the exploration of airfoil shaping by adding V shape to the existing NACA 0012. Through extensive simulations, analyses, and comparisons, valuable insights have been gained regarding the effects of these shaping on drag reduction, lift enhancement, flow separation, and other relevant aerodynamic parameters. One notable result of this research is the identification of the optimum V shape length of 23.33 mm, which exhibits drag reduction with 3.86% compared to the baseline NACA 0012 airfoil. However, further investigation is warranted to fully understand the underlying mechanisms and potential limitations associated with this specific configuration. Continued research and experimentation will provide deeper insights into the performance characteristics and optimal operating conditions of the V-shaped leading-edge morphing technique.

REFERENCES

[1.] Airfoil Tools, a. *NACA 4 digit airfoil generator (NACA 2412 AIRFOIL.* http://airfoiltools.com/airfoil/naca4digit
[2.] Airfoil Tools, b. *NACA 0012 AIRFOILS (n0012-il).* http://airfoiltools.com/airfoil/details?airfoil=n0012-il
[3.] *ANSYS FLUENT, 12.0. User's Guide-7.3.10, Inputs at Pressure Far-Field Boundaries.* https://www.afs.enea.it/project/neptunius/docs/fluent/html/ug/node246.htm
[4.] ANSYS, 2021. *Ansys Fluent Theory Guide*. https://dl.cfdexperts.net/cfd_resources/Ansys_Documentation/Fluent/Ansys_Fluent_Theory_Guide.pdf
[5.] El Maani, R., Radi, B., & El Hami, A. (2018). CFD Analysis of the Transonic Flow over a NACA 0012 Airfoil. *Incertitudes et Fiabilité Des Systèmes Multiphysiques*, *2*(2). doi: 10.21494/iste.op.2018.0307
[6.] Haygood, J. 2022. How angle of attack indicator works. https://www.skytough.com/post/how-angle-of-attack-indicator-works
[7.] Holst, T. L. (1988). *Computational Fluid Dynamics Drag Prediction-Results from the Viscous Transonic Airfoil Workshop.* https://ntrs.nasa.gov/search.jsp?R=19880012625
[8.] IPCC, (1999). the Global Atmosphere, edited by JE Penner, DH Lister, DJ Griggs, DJ Dokken, and M. McFarland, 370 pp.
[9.] James, L. T. (1986). Far-field boundary conditions for transonic lifting solutions to theEuler equations. *AIAA Journal*, *24*(7), 1074-1080.
[10.] LEAP CFD Team, 2012. *Tips & Tricks: Inflation Layer Meshing in ANSYS. https://www.computationalfluiddynamics.com.au/tips-tricks-inflation-layer-meshing-in-ansys/*
[11.] LEAP CFD Team, 2020. *What y+ should I use? Part 1 – Understanding the physics of boundary layers. https://www.computationalfluiddynamics.com.au/y-plus_part1_understanding-the-physics-of-boundary-layers/*
[12.] Leishman, J. G. (2023). Airplane Stability & Control. *Introduction to Aerospace Flight Vehicles*. doi: 10.15394/EAGLEPUB.2022.1066.N42
[13.] Menter, F.R., Lechner, R. and Matyushenko, A. Best Practice: RANS Turbulence Modeling in Ansys CFD. Version 1.0. https://www.ansys.com/resource-center/technical-paper/best-practice-rans-turbulence-modeling-in-ansys-cfd
[14.] NASA Glenn Research Center. Airplane parts and function. https://www1.grc.nasa.gov/beginners-guide-to-aeronautics/airplane-parts-function/
[15.] Norman, J. R. (1929). Note on a sailfish (Istiophorus americanus Cuvier and Valenciennes) new to the British fauna. *Journal of the Marine Biological Association of the United Kingdom*, *16*(1), 67-71.
[16.] Sagong, W., Jeon, W. P., & Choi, H. (2013). Hydrodynamic characteristics of the sailfish (Istiophorus platypterus) and swordfish (Xiphias gladius) in gliding postures at their cruise speeds. *PloS one*, *8*(12), e81323.
[17.] Thomas, J. L., & Salas, M. D. (1986). Far-field boundary conditions for transonic lifting solutions to theEuler equations. *AIAA journal*, *24*(7), 1074-1080. https://doi.org/10.2514/3.9394
[18.] Wood, A. 2022. *Aircraft Horizontal and Vertical Tail Design. Aerotoolbox.* https://aerotoolbox.com/design-aircraft-tail/
[19.] Martins, J. R. (2022). Aerodynamic design optimization: Challenges and perspectives. *Computers & Fluids*, *239*, 105391.
[20.] Tanarro, Á., Vinuesa, R., & Schlatter, P. (2020). Effect of adverse pressure gradients on turbulent wing boundary layers. *Journal of Fluid Mechanics*, *883*, A8.
[21.] Neuenhahn, T., & Olivier, H. (2006). Influence of the wall temperature and the entropy layer effects on double wedge shock boundary layer interactions. In *14th AIAA/AHI space planes and hypersonic systems and technologies conference* (p. 8136).
[22.] Jang, K. S., Le, T. T. G., Kim, J., Lee, K. S., & Ryu, J. (2021). Effects of compressible flow phenomena on aerodynamic characteristics in Hyperloop system. *Aerospace Science and Technology*, *117*, 106970.
[23.] Sundharasan, R., Gowtham, G., Kumaran, T., & Elumalai, K. (2022). Aerodynamics Enhancement Using Adaptive Flow Control. In *Handbook of Research on Aspects and Applications of Incompressible and Compressible Aerodynamics* (pp. 323-342). IGI Global.
[24.] Clemens, N. T., & Narayanaswamy, V. (2014). Low-frequency unsteadiness of shock wave/turbulent boundary layer interactions. *Annual Review of Fluid Mechanics*, *46*, 469-492.
[25.] Liem, R. P., Mader, C. A., & Martins, J. R. (2015). Surrogate models and mixtures of experts in

aerodynamic performance prediction for aircraft mission analysis. *Aerospace Science and Technology*, *43*, 126-151.

[26.] Placek, R., & Ruchała, P. (2018). The flow separation development analysis in subsonic and transonic flow regime of the laminar airfoil. *Transportation Research Procedia*, *29*, 323-329.

[27.] Nejati, A., & Mazaheri, K. (2016). Drag reduction by a multi-point optimised hybrid flow control method for two supercritical airfoils. *European Journal of Computational Mechanics*, *25*(5), 359-387.